Cell

Reversal of Histone Lysine Trimethylation by the JMJD2 Family of Histone Demethylases

Johnathan R. Whetstine,[1] Amanda Nottke,[1] Fei Lan,[1] Maite Huarte,[1] Sarit Smolikov,[2] Zhongzhou Chen,[3] Eric Spooner,[4] En Li,[5] Gongyi Zhang,[3] Monica Colaiacovo,[2] and Yang Shi[1,*]

[1] Department of Pathology
[2] Department of Genetics
Harvard Medical School, 77 Avenue Louis Pasteur, Boston, MA 02115, USA
[3] Integrated Department of Immunology, National Jewish Medical and Research Center, University of Colorado
Health Science Center, Denver, CO 80206, USA
[4] Whitehead Institute, Nine Cambridge Center, Massachusetts Institute of Technology, Cambridge, MA 02142, USA
[5] Novartis Biomedical Research Institute, Cambridge, MA 02142, USA
*Contact: yang_shi@hms.harvard.edu

SUMMARY

Histone methylation regulates chromatin structure, transcription, and epigenetic state of the cell. Histone methylation is dynamically regulated by histone methylases and demethylases such as LSD1 and JHDM1, which mediate demethylation of di- and monomethylated histones. It has been unclear whether demethylases exist that reverse lysine trimethylation. We show the JmjC domain-containing protein JMJD2A reversed trimethylated H3-K9/K36 to di- but not mono- or unmethylated products. Overexpression of JMJD2A but not a catalytically inactive mutant reduced H3-K9/K36 trimethylation levels in cultured cells. In contrast, RNAi depletion of the *C. elegans* JMJD2A homolog resulted in an increase in general H3-K9Me3 and localized H3-K36Me3 levels on meiotic chromosomes and triggered p53-dependent germline apoptosis. Additionally, other human JMJD2 subfamily members also functioned as trimethylation-specific demethylases, converting H3-K9Me3 to H3-K9Me2 and H3-K9Me1, respectively. Our finding that this family of demethylases generates different methylated states at the same lysine residue provides a mechanism for fine-tuning histone methylation.

INTRODUCTION

The N-terminal tails of histones are subject to a plethora of posttranslational modifications including phosphorylation, ubiquitination, acetylation, and methylation. Each modification can affect chromatin architecture, but the total sum of these modifications may be the ultimate determinant of the chromatin state, which governs gene transcription (Jenuwein and Allis, 2001; Strahl and Allis, 2000). Histone methylation has been implicated in multiple biological processes including heterochromatin formation, X-inactivation, genomic imprinting, and silencing of homeotic genes (Kouzarides, 2002; Lachner and Jenuwein, 2002; Margueron et al., 2005; Martin and Zhang, 2005). Aberrant histone methylation has been linked to a number of human diseases such as cancer (Fraga et al., 2005; Hake et al., 2004; Schneider et al., 2002; Varambally et al., 2002; Hess, 2004a; Okada et al., 2005). Methylation occurs on both lysine (K) and arginine (R) residues. Five K residues on the tails of histone H3 and H4 (H3-K4, H3-K9, H3-K27, H3-K36, and H4-K20) as well as K79 located within the core of histone H3 have been shown to be sites for methylation (Margueron et al., 2005; Zhang and Reinberg, 2001). Methylation at these sites has been linked to both transcriptional activation and repression, as well as DNA-damage response (Sanders et al., 2004; Zhang and Reinberg, 2001), demonstrating a widespread role for histone methylation in various aspects of chromatin biology (Martin and Zhang, 2005). Lysine residues can be mono-, di-, or trimethylated. These differentially methylated lysine residues may serve as docking sites for different effector proteins and/or platforms for chromatin modifiers including histone methylases, deacetylases, or remodeling activities, which may result in potentially diverse functional outcomes and underscore the complexity of methylation regulation.

Euchromatic histone methylation can contribute to either transcriptional activation or repression. In general, methylation at histone H3-K4 and H3-K36, including di- and trimethylation at these sites, has been linked to actively transcribed genes (reviewed in Martin and Zhang [2005]). In contrast, H3-K9 promoter methylation is

considered a repressive mark for euchromatic genes (Nielsen et al., 2001; Shi et al., 2003) and is also one of the landmark modifications associated with heterochromatin (Nakayama et al., 2001; Peters et al., 2002; Rea et al., 2000). Interestingly, a recent study identified association of H3-K9 trimethylation (H3-K9Me3) with actively transcribed genes as well (Vakoc et al., 2005). The difference appears to lie in the location of H3-K9Me3, i.e., actively transcribed genes are enriched for H3-K9Me3 within the coding region (Vakoc et al., 2005). Thus, methylation at different lysine residues, degrees of methylation at the same lysine residue, as well as the locations of the methylated histone within a specific gene locus, can impact transcriptional and biological outcomes.

Unlike other histone modifications such as acetylation, methylation has long been considered a "permanent" modification. This view was based on the earlier observation that the half-lives of histones and total histone methyl groups were comparable, which led to the conclusion that histone methylation is stable and irreversible (Byvoet et al., 1972; Thomas et al., 1972). However, the identification of the H3-K4-specific histone demethylase LSD1 challenged this view and suggested that histone methylation is reversible and dynamically regulated (Shi et al., 2004). When in complex with the androgen receptor, LSD1 has also been shown to demethylate H3-K9Me2, expanding the substrate repertoire of LSD1 (Metzger et al., 2005). The LSD1 protein interactions have also been shown to play a key role in either facilitating or inhibiting demethylation of more complex substrates (Lee et al., 2005; Shi et al., 2005). Importantly, the finding that LSD1 mediates demethylation via a FAD-dependent oxidative reaction predicts that nuclear proteins that are capable of mounting an oxidative reaction of the N-methylated proteins are possible candidates for histone demethylases (Shi et al., 2004). Consistent with this, a second histone demethylase, JHDM1, has been recently reported (Tsukada et al., 2006). JHDM1 specifically demethylates H3-K36Me2 via an oxidative reaction catalyzed by the evolutionarily conserved JmjC domain, although the detailed chemical mechanism differs from that of LSD1 (Tsukada et al., 2006). Both LSD1 and JHDM1 demethylate only di- or monomethylated histones. The inability of LSD1 to demethylate trimethylated histone is due to its inherent chemistry, i.e., LSD1 requires protonated nitrogen in the substrate for the demethylation reaction to occur, thus precluding trimethylated proteins as its substrates. JHDM1, however, uses Fe(II) and α-ketoglutarate as cofactors to mediate a hydroxylation-based demethylation and therefore does not require protonated nitrogen for demethylation. The basis for the preference of JHDM1 for mono- and di- but not trimethylated substrates remains to be determined. Collectively, these findings raise the possibility that trimethylation either represents a permanent modification or its reversal may involve yet-to-be-identified histone demethylases.

The JmjC domain is conserved from bacteria to eukaryotes and belongs to the cupin superfamily of metalloenzymes. There are over 100 JmjC domain proteins across the evolutionary phyla and essentially all of them are predicted to be enzymes (Clissold and Ponting, 2001). JmjC domains can mediate radical-based oxidative reactions (hydroxylation) and are chemically compatible with demethylation of trimethylated substrates. In search for a trimethylation-specific histone demethylase, we used a candidate approach and focused on approximately 28 human JmjC domain-containing proteins. In this report, we provide evidence that a subset of these JmjC proteins, i.e., the JMJD2 subfamily, are histone lysine trimethyl demethylases. The JMJD2 family is composed of four members (JMJD2A, JMJD2B, JMJD2C, and JMJD2D); Katoh, 2004). JMJD2A has recently been shown to interact with the tumor suppressor Rb, histone deacetylases (HDACs), and the corepressor N-CoR and functions as a repressor in part through the recruitment of HDACs and N-CoR, respectively (Gray et al., 2005; Yoon et al., 2003; Zhang et al., 2005). However, molecular mechanisms by which JMJD2A represses transcription are incompletely understood. JMJD2C is also known as GASC-1 (gene amplified in squamous cell carcinoma) and has been implicated in tumorigenesis (Yang et al., 2000). Essentially nothing was known about JMJD2B and JMJD2D.

We show that JMJD2A is a lysine trimethyl-specific histone demethylase, which catalyzes demethylation of H3-K9Me3 and H3-K36Me3, but not mono, di-, or trimethylated H3-K4, H3-K27, and H4-K20. JMJD2A converts H3-K9/36Me3 to H3-K9/36Me2 but not H3-K9/36Me1 or unmethylated products. Consistent with these observations, overexpression of JMJD2A results in a reduction of H3-K9/36Me3 in cultured cells. Furthermore, RNAi depletion of the *C. elegans* JMJD2A homolog (*ceJMJD2*) causes a localized H3-K36Me3 increase on the X chromosome and higher H3-K9Me3 levels on meiotic chromosomes in the adult hermaphrodite germline. In addition, we observed increased germ cell apoptosis consistent with the activation of a DNA-damage checkpoint. Collectively, these findings provide strong evidence that JMJD2A is a lysine trimethyl-specific demethylase that may play an important role in development. We further demonstrated that the other human JMJD2 family members are mainly trimethyl-specific histone demethylases as well. Our findings identify a family of enzymes that specifically reverse trimethylated histones and demonstrate the importance of these enzymes in a multicellular organism.

RESULTS

JMJD2A Is a KMe3-Specific Demethylase

JMJD2A is a member of the JMJD2 subfamily of JmjC domain-containing proteins and is evolutionarily conserved from *C. elegans* to human (Figure 1). All four members contain the JmjC domain, which is predicted to be a metalloenzyme catalytic motif (Clissold and Ponting, 2001). JMJD2E and -2F were previously reported to be members of this family (Katoh, 2004), which are intronless genes
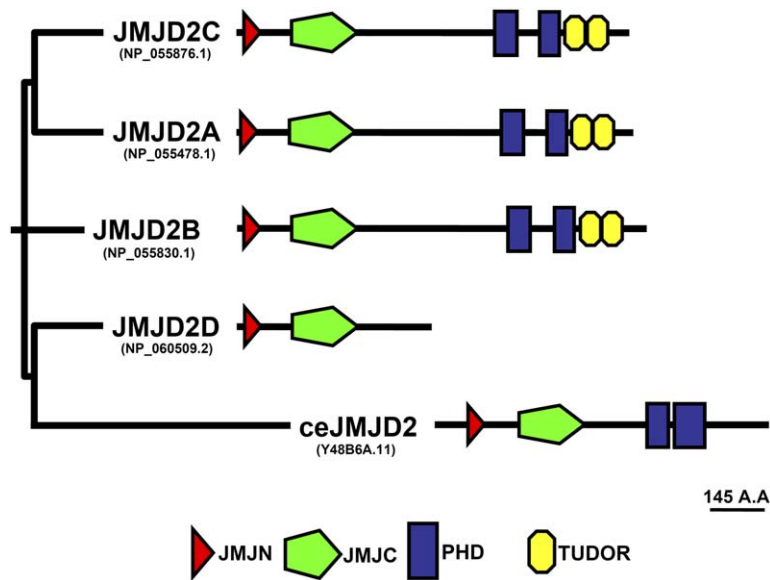
located adjacent to *jmjd2d*. It remains unclear whether they are functional genes as they are not represented by any current human ESTs. The JMJD2 family members also contain the JmjN domain, which is conserved among a subset of JmjC domain proteins. With the exception of JMJD2D, the other three members contain two PHD and Tudor domains, which are found in many proteins associated with chromatin and transcriptional regulation. The Tudor domain of JMJD2A has recently been shown to bind H3-K4Me3, H3-K9Me3, as well as H4-K20Me3 and H4-K20Me2 in vitro (Kim et al., 2006); however, the functional significance of this binding remains unclear. Phylogenic analysis of the first 350 amino acids for this subfamily, which contain both the JmjN and JmjC domains, shows that JMJD2A and -2C are more similar to one another than JMJD2B and -2D. They all contain the conserved amino acids that are associated with Fe(II) coordination (see Figure S1 in the Supplemental Data available with this article online; Lee et al., 2003).

To determine whether JMJD2A is a histone demethylase, we isolated a full-length JMJD2A cDNA from HeLa cells by RT-PCR, subcloned it into a Gateway entry vector, and subsequently transferred it to expression vectors used to purify the recombinant protein from insect Sf9 cells to near homogeneity (Figure S2). In order to determine whether JMJD2A had histone demethylase activity, we used a MALDI-TOF mass spectrometric approach to screen for demethylation using a variety of histone peptides representing mono-, di-, and trimethylation for at least five different H3 lysine residues. With this approach, we were able to detect enzymes with low levels of demethylation activity. As shown in Figure 2, JMJD2A mediated demethylation at two of the five sites tested, namely H3-K9 and H3-K36, but not H3-K4, H3-K27, and H4-K20. Importantly, JMJD2A appeared to specifically demethylate H3-K9Me3 and H3-K36Me3 (Figure 2, shaded panels),

but not H3-K9/K36Me2 or H3-K9/K36Me1. Furthermore, the demethylation reaction of H3-K9Me3 and H3-K36Me3 only resulted in dimethylated, but no mono- or un-methylated products (Figure 2).

JmjC domain-mediated demethylation reactions require Fe(II) and α-ketoglutarate as cofactors (Tsukada et al., 2006). As shown in Figure 3, consistent with the proposed chemistry, omission of α-ketoglutarate or addition of the iron chelator deferoxamine (DFO; 250 μM) completely inhibited the demethylation reactions mediated by JMJD2A at both the H3-K9 and H3-K36 sites. In addition, the N-terminal 350 amino acids of JMJD2A, which include both the JmjN and JmjC domains, are sufficient to mediate the demethylation reactions with the same site specificity as that of the full-length JMJD2A (Figures 3 and S3). Only when excess amounts of purified JMJD2A protein were used (75 μg) did we see low levels of demethylation of H3-K9Me2 or H3-K36Me2 (data not shown). Consistent with these observations, when using bulk histones as substrates, Western blot analysis also showed robust JMJD2A-mediated demethylation at both H3-K9Me3 and H3-K36Me3, but not H3-K9Me2 or H3-K36Me2. However, we also noticed a slight decrease in H3-K4me3 using the same assay conditions (Figure 3B). The JMJD2A fragment (1–350 aa) was able to demethylate histones but required more enzyme (at least 3-fold) to achieve a similar decrease in H3-K9Me3 and H3-K36Me3 signals (data not shown).

As discussed earlier, JmjC domain-containing proteins belong to the cupin superfamily of metalloenzymes. Three amino acids predicted to be involved in metal binding are conserved in almost all JmjC domain proteins (Clissold and Ponting, 2001). In JMJD2A, these three amino acids are His 188, Glu 190, and His 276. Consistently, mutation of H188 to alanine (A) essentially abrogated the demethylase activity of JMJD2A (Figure 3A). Taken together, our
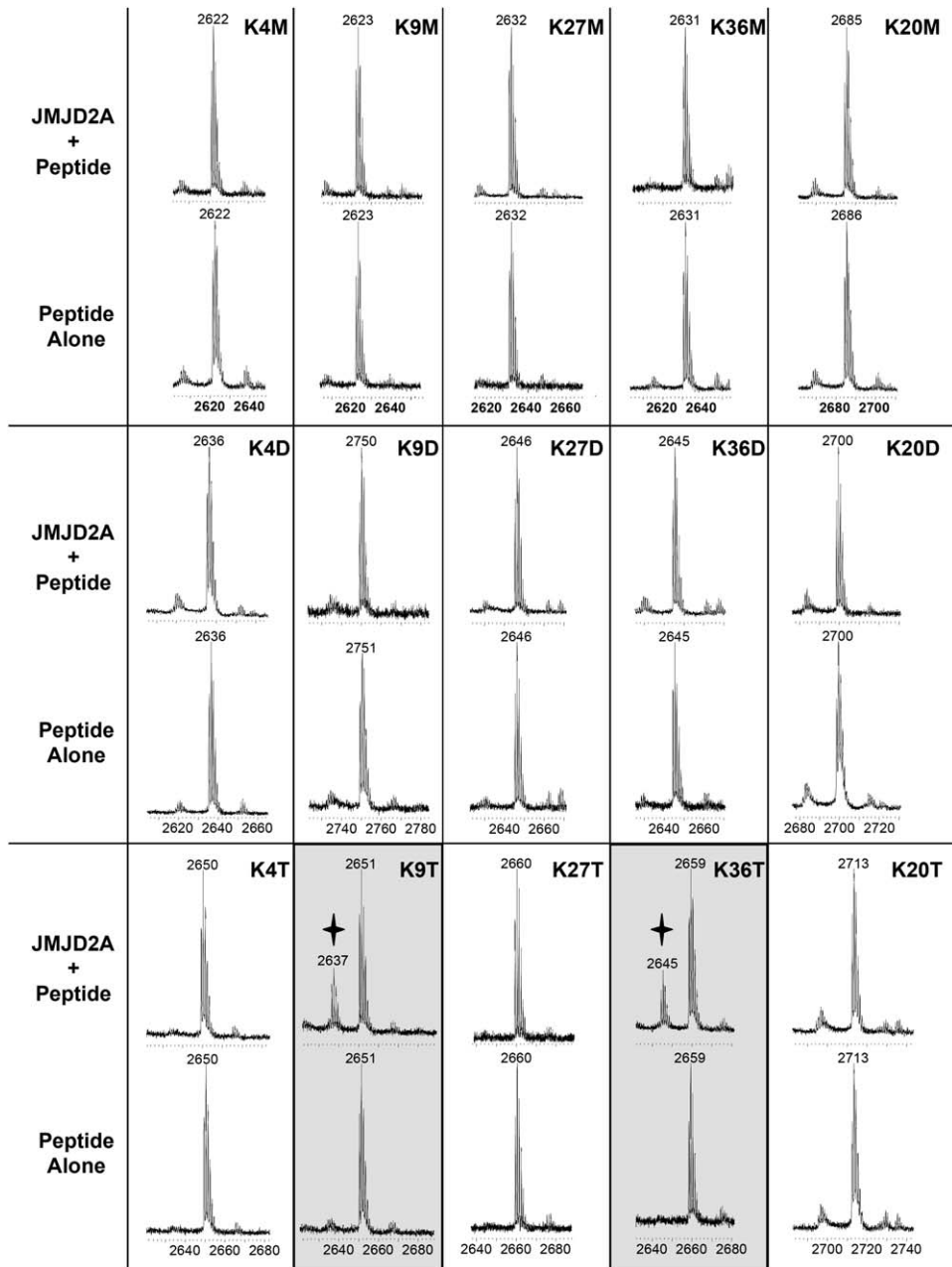
Figure 2. Identification of Histone Demethylase Activity for Full-Length JMJD2A by MALDI-TOF Mass Spectrometry
Each panel contains spectrum for either mono- (M), di- (D), or trimethylated (T) peptides (histone 3 lysines 4, 9, 27, 36, or histone 4 lysine 20; 10 μM) incubated alone or with full-length JMJD2A (1–2 μg). The appearance of a peak corresponding to demethylated peptide is marked with a star and a shaded panel. The shift corresponds to a loss of 14 Da because $-CH_3$ is removed and a $-H$ is added. Only trimethylated lysines 9 and 36 were demethylated by full-length JMJD2A.

in vitro analysis indicates that JMJD2A functions as a histone H3-K9/36Me3 demethylase.

JMJD2A Overexpression Antagonizes H3-K9Me3 and H3-K36Me3 In Vivo

We next determined whether JMJD2A overexpression would alter H3-K9 and H3-K36 trimethylation in vivo.

JMJD2A was tagged with the HA epitope (HA-JMJD2A) and transfected into HeLa cells. Forty-eight hours posttransfection, cells were fixed and costained with antibodies recognizing the HA epitope and histone methylation at various lysine residues. As shown in Figures 4A–4D, the signal representing H3-K36Me3 was significantly reduced in cells where HA-JMJD2A was either highly or
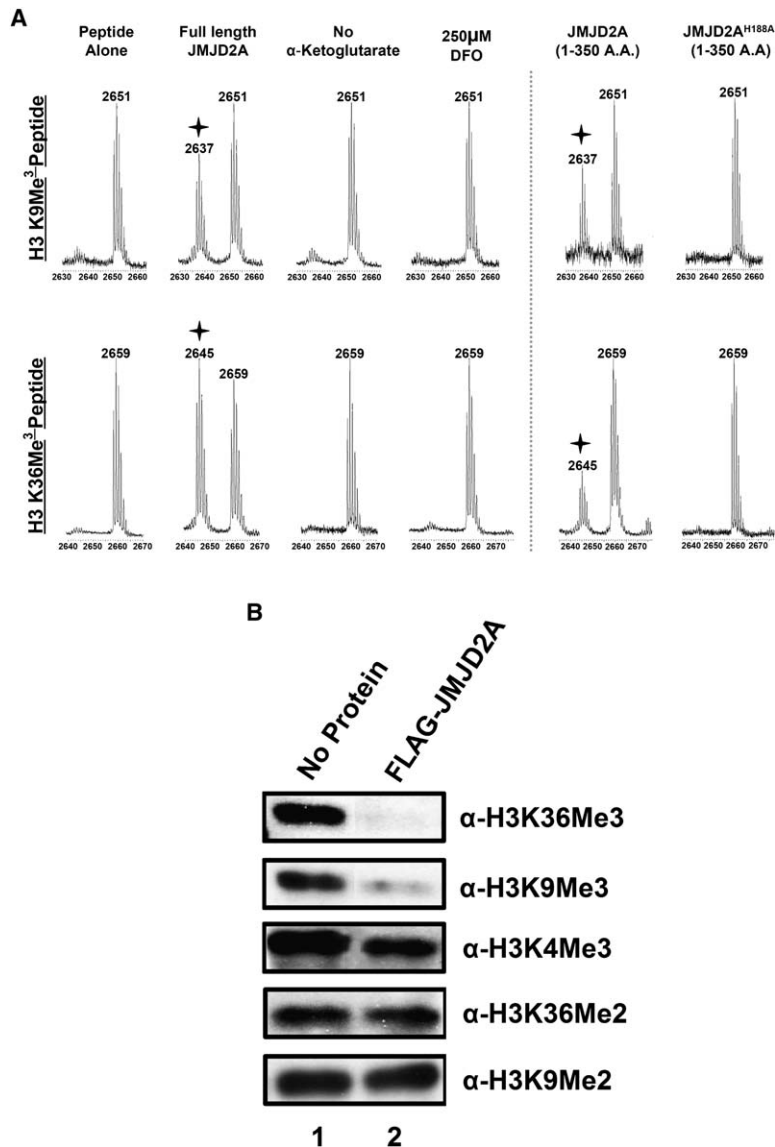
A

Figure 3. Catalytic Activity of Full-Length hJMJD2A and JmjN/JmjC Domains for JMJD2A Requires Fe(II) and α-Ketoglutarate

(A) The full-length protein does not demethylate either trimethylated lysine 9 or 36 when α-ketoglutarate is omitted from the reaction. The truncated protein also requires α-ketoglutarate (data not shown). The divalent chelator EDTA (10 μM; data not shown) and iron-specific poison DFO (250 μM) inhibit the demethylation reaction. Histidine 188 was predicted to interact with Fe(II) and when mutated (histidine to alanine; H188A) demethylase activity was abrogated.

(B) The full-length JMJD2A demethylates histone 3 K9/36Me3 in vitro. Histone (5 μg) was incubated with 1 μg of full-length JMJD2A in the demethylase reaction buffer for 4 hr at 37°C. Equal amounts from each reaction were probed with H3 antibodies to H3-K4Me3, H3-K9Me2, H3-K9Me3, H3-K36Me2, and H3-K36Me3.

B

moderately overexpressed (marked by arrows). We counted 166 transfected cells and found that H3-K36Me3 levels decreased in approximately 63% of these cells (104/166 cells; Table 1). As a control, we also examined 50 surrounding nontransfected cells and found that the majority of these cells (90%; 45/50 cells) showed no change in H3-K36Me3 levels (Table 1). Similarly, we also observed a significant decrease in H3-K9Me3 level in the HA-JMJD2A transfected cells (44% [55/124 cells]; Figures 4E–4H; Table 1). No overt changes were observed for monomethylated H3-K9/36 as a result of overexpression of JMJD2A; however, mild increases in dimethyl histone 3 K9/36 were observed (3.1- and 1.6-fold, respectively; Table 1). As a further control, we showed that the H3-K4Me3 signal was essentially unaffected, indicating substrate specificity (Figures 4I–4L; 0/126 cells). Importantly, the point mutation H188A that abrogated the demethylase

activity of JMJD2A (Figure 3A) eliminated the ability of HA-JMJD2A to reduce H3-K9/36 trimethylation in vivo (6/80 and 1/74 cells, respectively; Table S1), suggesting that the loss of the trimethylation signals was likely due to demethylation (Figures 4M–4P). Taken together, these findings provide in vivo evidence that JMJD2A antagonize trimethylation at H3-K9 and H3-K36, likely via enzymatic demethylation.

RNAi-Mediated Depletion of the *C. elegans* JMJD2A Homolog Results in Increased H3-K36Me3 and H3-K9Me3 Levels in the Adult Germline

To further examine whether JMJD2A affects H3-K9/36 trimethyl demethylation in vivo, we analyzed the highly conserved *C. elegans* homolog (*Y48B6A.11*). In *C. elegans*, there are two JmjN/JmjC domain-containing proteins. Only Y48B6A.11 is a member of the JMJD2 family and
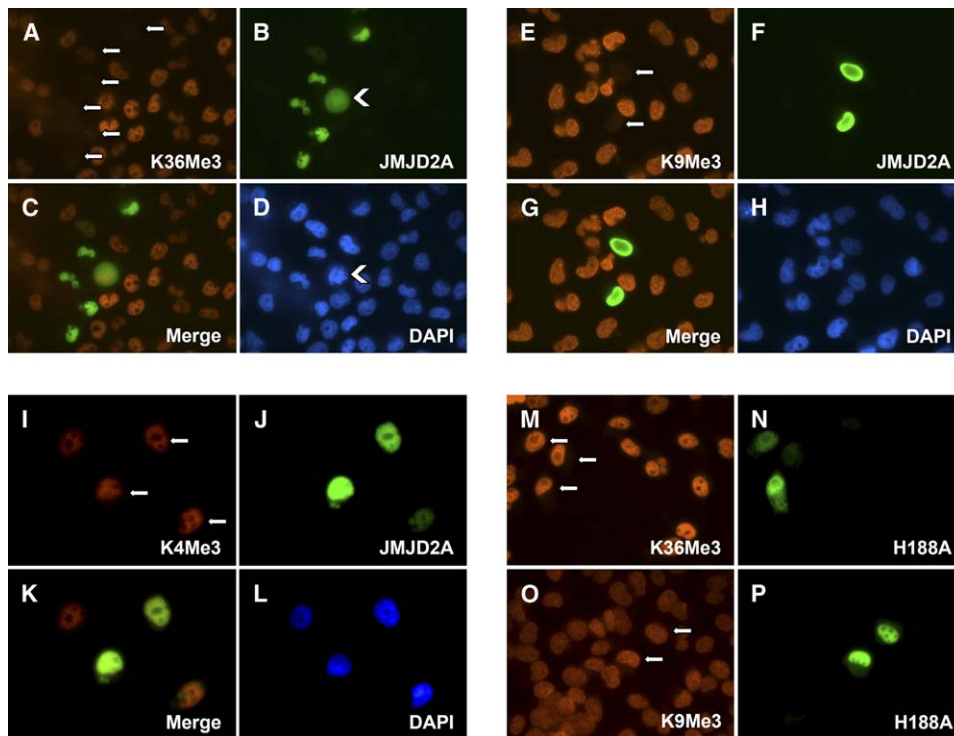
Figure 4. Overexpression of Full-Length hJMJD2A Results in Decreased H3-K9Me3 and H3-K36Me3 in HeLa Cells

(A–D) Moderate to high overexpression of HA-tagged JMJD2A causes decreased levels of H3-K36Me3. The loss of H3-K36Me3 is indicated with an arrow. The demethylation activity was lost when histidine 188 was mutated to alanine (H188A; [M] and [N]). HA-JMJD2A relocalizes during mitosis (arrowhead, [A]).

(E–H) High levels of HA-JMJD2A cause a loss of H3-K9Me3 in HeLa cells. The loss of K9Me3 is marked with arrows. The effect that HA-JMJD2A had on H3-K9Me3 was lost when histidine 188 was mutated to alanine (H188A; [O] and [P]).

(I–L) Overexpression of HA-JMJD2A had no effect on histone 3 lysine 4 trimethylation in HeLa cells. The green corresponds to anti-HA; the red corresponds to the specific antibody; the blue corresponds to DAPI. The effect of HA-JMJD2A was specific for H3-K9/36Me3 (see Tables 1 and 2).

has a high sequence and domain similarity to JMJD2A-D (named *ceJMJD2*; Figures 1 and S1). We developed an RNAi feeding strategy that successfully knocked down *ceJMJD2* transcripts (Figure S4A) and observed an increase in germ cell apoptosis (section below). Since the *C. elegans* germline was affected by the depletion of *ceJMJD2*, we investigated whether there were alterations in both K9Me3 and K36Me3 in the germline of *ceJMJD2 (RNAi)* animals. In wild-type N2 worms, H3-K36Me3 staining is observed over the entire length of the autosomes throughout meiotic prophase. H3-K36Me3 staining on the X chromosome tip occurred infrequently and was restricted to one end during early meiotic prophase (i.e., transition zone to mid-pachytene nuclei). During late-pachytene and early-diplotene, staining of the X becomes gradually more extensive, eventually completely extending along the entire length of the X chromosome in all meiocytes (data not shown). We confirmed the X chromosome identity by using combined anti-H3-K36Me3, DAPI, and X FISH probe staining (Figure S4C). In the *ceJMJD2 (RNAi)* animals, we observed a 3-fold increase in the number of mid-pachytene nuclei carrying H3-K36Me3 staining

on the tip of the X chromosome (zone 5; Figure S4B; n = 83/117, where n = number of nuclei carrying a stained X chromosome/total number of nuclei analyzed) when compared with the controls (n = 31/123; Figures 5A and 5B).

In addition to the localized, increased frequency of H3-K36Me3 X chromosome staining, we observed an increase in H3-K9Me3 signal in all meiocytes throughout prophase (Figure 5C and data not shown). Wild-type or *control (RNAi)* worms have a limited number of H3-K9Me3 foci, whereas *ceJMJD2 (RNAi)* worms had more abundant, broadly distributed H3-K9Me3 foci along the chromosomes in the germline nuclei (Figure 5C). We also noted significantly more condensed nuclei (as determined by DAPI stained morphology) with high levels of H3-K9Me3 staining at late-pachytene (Figures 5C and 5D; arrow). The condensed nuclei occurred at a higher frequency upon *ceJMJD2 (RNAi)*, as many as thirteen times per gonad arm. In contrast, the number of condensed nuclei in the control gonad arms never exceeded five per gonad (Figure 5D). We stained for H3-K9Me2 and did not observe significantly different patterns or levels in RNAi treated worms (data not shown).

Table 1. JMJD2A Overexpression Results in Decreased Histone 3 Lysine 9 and 36 Trimethylation

	Mono-		Di-		Tri-	
	HA-JMJD2A	No Expression	HA-JMJD2A	No Expression	HA-JMJD2A	No Expression
Histone 3 Lysine 36 Methylation						
No change	93.0% (80/86)	91.9% (57/62)	87.7% (128/146)	92.3% (60/65)	33.70% (56/166)	82% (41/50)
Increase	7.0% (6/86)	6.5% (4/62)	12.3% (18/146)	7.7% (5/65)	3.70% (6/166)	8% (4/50)
Decrease	0% (0/86)	1.6% (1/62)	0% (0/146)	0% (0/65)	62.70% (104/166)	10% (5/50)
Histone 3 Lysine 9 Methylation						
No change	97.3% (106/109)	96.5% (55/57)	81.3% (126/155)	94.0% (47/50)	54.8% (68/124)	100% (50/50)
Increase	0.9% (1/109)	3.5% (2/57)	18.7% (29/155)	6.0% (3/50)	0.8% (1/124)	0% (0/50)
Decrease	1.8% (2/109)	0% (0/57)	0% (0/155)	0% (0/50)	44.6% (55/124)	0% (0/50)
Histone 3 Lysine 4 Methylation						
No change	96.2% (49/51)	96.8% (62/64)	97.3% (109/112)	98.0% (98/100)	98.4% (124/126)	100% (50/50)
Increase	1.9% (1/51)	1.6% (1/64)	2.7% (3/112)	2.0% (2/100)	1.6% (2/126)	0% (0/50)
Decrease	1.9% (1/51)	1.6% (1/64)	0% (0/112)	0% (0/100)	0% (0/126)	0% (0/50)

Cells were transfected with a HA-tagged JMJD2A for 48 hr before being fixed, stained for the indicated antibodies, and analyzed by fluorescence microscopy. Cells that were expressing moderate to high levels were scored for the level of histone 3 K4, 9, and 36 methylation (mono-, di-, and tri-). At the same time, nontransfected cells on the same slide were counted for changes in methylation status as well.

Depletion of *ceJMJD2* Increases Germline Apoptosis and RAD-51 Staining

The condensed nuclei, based on their DAPI-stained appearance, levels, and location in the *C. elegans* germline have been previously attributed to germ cell apoptosis (Gumienny et al., 1999; Colaiacovo et al., 2003). For this reason, we further tested the effect of *ceJMJD2* depletion on germ cell apoptosis in *C. elegans*. Using both Nomarski optics and acridine orange (AO) staining, the total number of germ cell corpses in the late-pachytene region were scored (Figures 6A–6I). The control treated worms had a normal level of germ cell death (3.32 ± 0.21 germ cell corpses/gonad arm; Gumienny et al., 1999); however, in contrast, the age-matched RNAi-treated worms had 9.24 ± 0.39 germ cell corpses/gonad arm (~3-fold increase, p < 0.0001; Figures 6A–6I).

DNA damage resulting from unrepaired meiotic double-strand breaks (DSBs) or genotoxic stress has been previously shown to trigger a pachytene DNA-damage checkpoint leading to increased germ cell apoptosis in late-pachytene (Gartner et al., 2000). In the *C. elegans* germline, DNA damage-induced, but not physiological apoptosis, requires the functional p53 homolog, CEP-1 (Derry et al., 2001; Schumacher et al., 2001; Schumacher et al., 2005). We found that the significant increase in apoptosis observed with *ceJMJD2 (RNAi)* was abrogated in the *cep-1 (lg12501)* deletion mutant (Schumacher et al., 2005), suggesting a link between ceJMJD2 and DNA damaged-induced apoptosis (*cep-1 (lg12501)*; *control (RNAi)* had 3.15 ± 0.27 germ cell corpses/gonad arm and *cep-1 (lg12501)*; *ceJMJD2 (RNAi)* had 3.5 ± 0.28 germ cell corpses/gonad arm; Figure 6I).

Given that we observed increased H3-K9Me3 and -K36Me3 staining in the pachytene regions typically associated with meiotic DSB repair and concomitant increase in p53-dependent germ cell apoptosis, we next investigated the possibility that depletion of ceJMJD2 by RNAi may have contributed to an increase in DSB or delayed repair by examining the number of RAD-51 foci per nucleus at mid-pachytene (Colaiacovo et al., 2003). RAD-51 is a member of the highly conserved RecA protein family involved in strand invasion/exchange during DSB repair (Rinaldo et al., 1998; Takanami et al., 1998; Sung, 1994). Given that RAD-51 associates with 3′ ssDNA overhangs after DSB formation, RAD-51 foci reflect nascent recombination intermediates. Analysis of both RAD-51 levels and temporal distribution throughout the germline allows for monitoring the progression of meiotic recombination (Alpi et al., 2003; Colaiacovo et al., 2003). As shown in Figure 6, there was a significant increase in the percentage of nuclei in mid-pachytene that contained a higher number of RAD-51 foci (Figures 6J–6L). We observed as many as 22 RAD-51 foci per nucleus in the RNAi treated worms (with 47.3% of the 165 nuclei examined carrying ≥9 RAD-51 foci/nucleus) compared with three to eight RAD-51 foci per nucleus in the control animals (with only 26.8% of the 184 nuclei examined carried ≥9 RAD-51 foci/nucleus; Figure 6L). The elevated RAD-51 foci levels may reflect either an increase in the levels of DSBs or a delay in repair. As in the control, the number of RAD-51 foci decreased in *ceJMJD2 (RNAi)* worms during late-pachytene. Moreover, RAD-51 foci were no longer apparent in either early diplotene or diakinesis oocytes (data not shown), which suggests that DSBs were eventually being repaired.
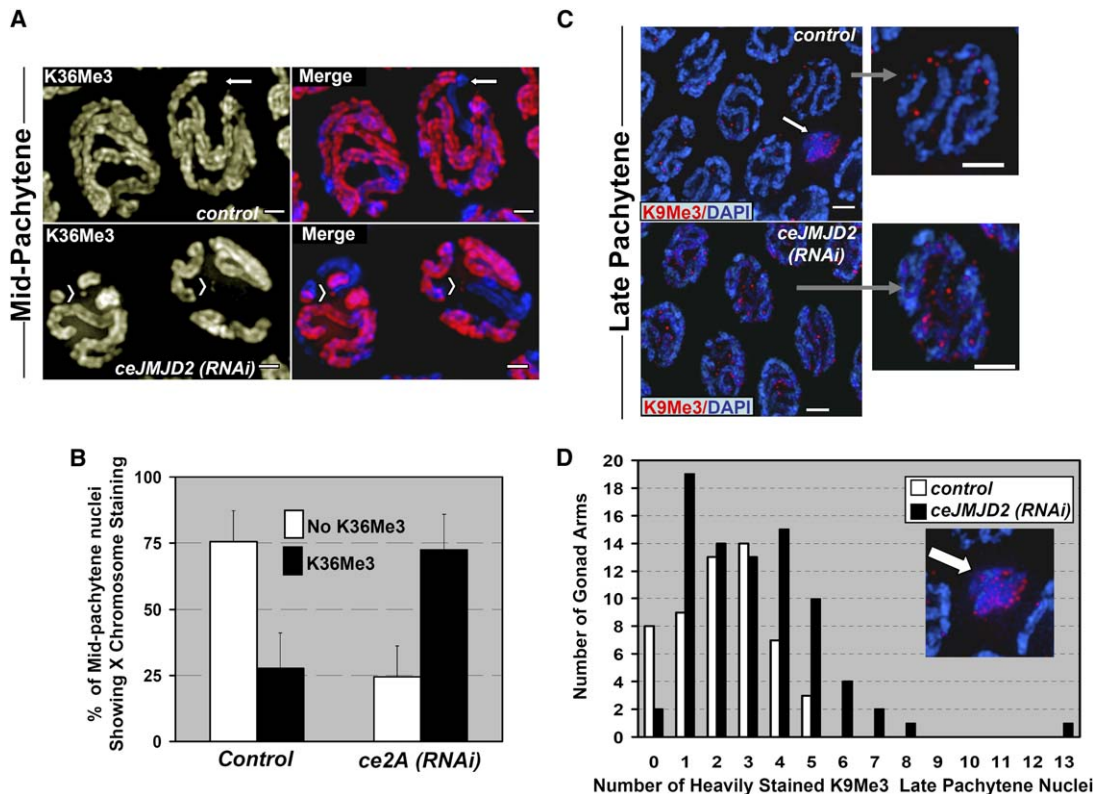
Figure 5. Depletion of the *C. elegans* JMJD2A Homolog Y48B6A.11 Increases Trimethylated Histone 3 lysine 9 and 36 In Vivo

(A) After *ceJMJD2 (RNAi)*, the frequency of X chromosome H3-K36Me3 staining increases in mid-pachytene nuclei. The left upper and lower panels are high magnification images of the mid-pachytene nuclei that are stained with anti-K36Me3 alone. The right panels show a merge of DAPI (blue) and anti-K36Me3 (red). The arrow indicates the unstained X chromosome in the control. Arrowheads indicate the stained X chromosome tip in RNAi-treated worms.

(B) A graphical representation of the increased percentage of X chromosome staining in mid-pachytene nuclei in *ceJMJD2 (RNAi)* worm gonads.

(C) Depletion of *ceJMJD2* results in a concomitant increase in H3-K9Me3 foci throughout germline nuclei. These panels show late-pachytene nuclei from either control or RNAi-treated worms stained with DAPI (blue) and anti-H3-K9Me3 (red). Enlarged nuclei are shown to the right of each panel. RNAi cells have more abundant H3-K9Me3 foci throughout the nuclei. The condensed nuclei with increased H3-K9Me3 staining are shown with an arrow in the control image.

(D) Graphical representation of the levels of condensed nuclei with intense K9Me3 staining (red) observed at late-pachytene. An enlarged view of this type of nuclei can be seen in the inset indicated with an arrow. The graph demonstrated a rightward shift in the number of condensed and heavily H3-K9Me3 stained nuclei per gonad after RNAi. As many as 13 nuclei/gonad arm were seen in the RNAi treated worms, which contrasted with the 5 nuclei/germline seen in control worms. Scale bar equals 2 μm.

Consistently, there was no evidence of chromosome fragmentation in oocytes undergoing diakinesis and all six chromosome pairs remained attached through chiasmata, indicating successful crossover formation (data not shown). Taken together, we demonstrated that alterations in the H3-K9 and -K36 trimethylation status in the *ceJMJD2 (RNAi)* germline coincides with significantly increased CEP-1/p53-dependent germ cell apoptosis and altered progression of meiotic DSB repair.

Demethylation by Other Members of the JMJD2 Family

The finding that human JMJD2A is a histone demethylase prompted us to investigate whether the other three closely related family members in human, JMJD2B, JMJD2C, and JMJD2D are histone lysine demethylases as well. The cDNAs encoding the first 350 amino acids of JMJD2B, -2C, and -2D, which include both the JmjN and JmjC domains (Figures 1 and S1), were subcloned into a HIS epitope-tag expression vector and purified from bacteria. As shown in Figure S5, mass spectrometry analysis revealed demethylation of H3-K9Me3 mediated by JMJD2C and JMJD2D but very weak demethylation by JMJD2B. JMJD2C also exhibited demethylation activity toward H3-K36Me3, but none of these proteins showed any activity toward other methylated sites including H3-K4, H3-K27, H3-K79, and H4-K20 (Figure S5 and data not shown). While JMJD2C only generated H3-K9Me2, JMJD2D converted H3-K9Me3 to H3-K9Me2 and H3-K9Me1. Consistently, JMJD2D was the only member that demethylated H3-K9Me2. Under our assay conditions, we never observed complete demethylation of the substrates. The
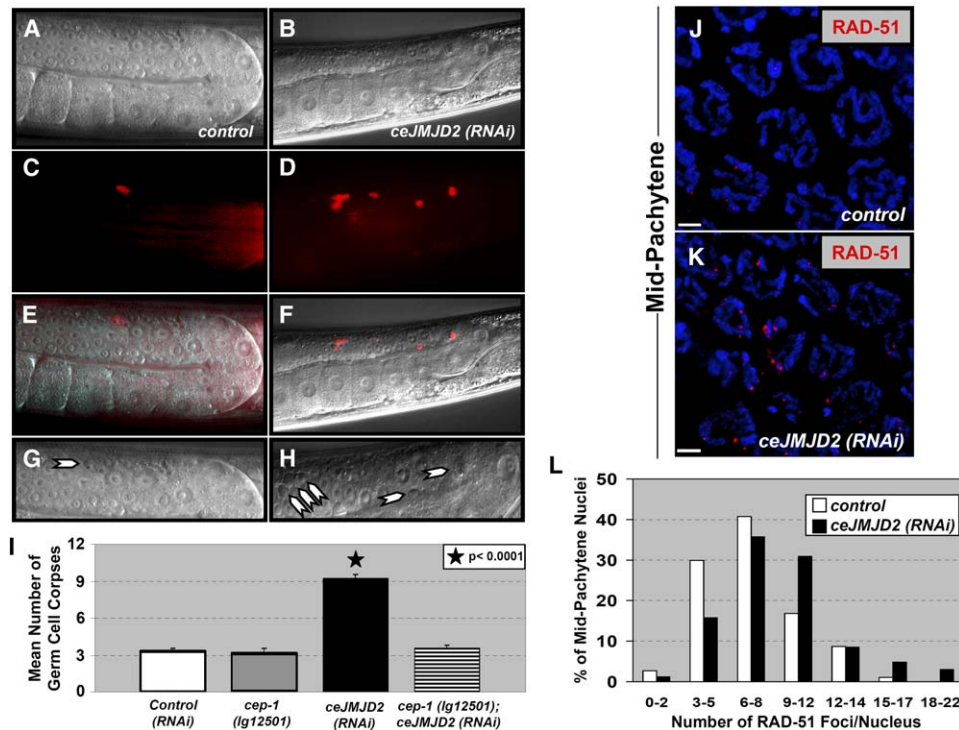
Figure 6. Depletion of *ceJMJD2* Leads to Increased Apoptosis and Elevated Levels of RAD-51 Foci

(A–I) Depletion of ceJMJD2 caused a significant increase in the number of germ cell corpses observed at late pachytene. Nomarski optics view shows the germ cell corpses in both control ([A] and enlarged view in [G], arrow) and RNAi-treated worms ([B] and enlarged view in [H], arrows).

(C and D) There are increased numbers of acridine orange positive cells in RNAi-treated worms (D) compared to the control worms (C). (E and F) show a merge of the acridine orange staining on the Nomarski image.

(I) A graphical representation of the mean number of germ cell corpses from two to five separate experiments. There is a 2.8-fold increase in germ cell apoptosis in *ceJMJD2 (RNAi)*-treated worms ($p < 0.0001$); however, in the *cep-1 (lg12501)* strain, the amount of apoptosis was dramatically reduced.

(J–L) Levels of RAD-51 foci were elevated in mid-pachytene nuclei in *ceJMJD2 (RNAi)* worms.

(J and K) These panels represent mid-pachytene nuclei (zone 5; see Figure S5) from whole-mount preparations stained with DAPI (blue) and with RAD-51 (red).

(L) Graphical representation of the quantitation of the observed numbers of RAD-51 foci/nucleus in zone 5 for both control and RNAi animals. RNAi led to an observable increase in the overall percentage of nuclei with ≥ 9 RAD-51 foci compared to control.

results of these analyses are summarized in Table 2. In summary, we have demonstrated that the JMJD2 family members are histone demethylases that are mainly involved in demethylation of trimethylated H3-K9 and -K36.

DISCUSSION

Histone methylation represents a fascinating posttranslational modification with multiple layers of complexity that suggest a very important role in chromatin biology. We have provided a number of new and important insights into histone methylation regulation. First, we have shown that trimethylation is dynamically regulated by specific demethylases as previously described for di- and monomethylation (Shi et al., 2004; Tsukada et al., 2006). Second, we demonstrated that the JMJD2 family of proteins have the ability to generate different states of methylation at H3-K9 (di- versus monomethylation), suggesting a mechanism for fine-tuning histone methylation. Third, as

suggested by the findings in *C. elegans*, we have demonstrated that these proteins are likely to play important biological roles in multicellular organisms.

Dynamic Regulation of Histone Lysine Trimethylation by Demethylases

Multiple lines of evidence suggest that histone lysine trimethylation plays an important role in chromatin biology. Trimethylation at H3-K9 and H4-K20 has been shown to be associated with constitutive heterochromatin (Schotta et al., 2004b), while H3-K9Me2 and K9Me3, along with H3-K27Me3 have been associated with X inactivation (Bean et al., 2004; Cowell et al., 2002; Kelly et al., 2002; Reuben and Lin, 2002; Rougeulle et al., 2004; Plath et al., 2003). However, H3-K9Me3 in the gene-coding regions is associated with transcriptional elongation (Vakoc et al., 2005), while, H3-K36Me2/3 plays an important role in suppressing inappropriate transcription within the body of genes (Carrozza et al., 2005; Joshi and Struhl, 2005;

Table 2. JMJD2 Family Demethylate Histone 3 K9 and/or K36

	JMJD2A	JMJD2B	JMJD2C	JMJD2D
H3-K4Me3	–	–	–	–
H3-K4Me2	–	–	–	–
H3-K4Me1	–	–	–	–
H3-K9Me3	++	+	++	++
H3-K9Me2	+/–[a]	–	–	++
H3-K9Me1	–	–	–	–
H3-K27Me3	–	–	–	–
H3-K27Me2	–	–	–	–
H3-K27Me1	–	–	–	–
H3-K36Me3	++	–	++	–
H3-K36Me2	+/–[a]	–	–	–
H3-K36Me1	–	–	–	–
H3-K79Me3	–	–	–	–
H3-K79Me2	–	–	–	–
H3-K79Me1	–	–	–	–
H4-K20Me3	–	–	–	–
H4-K20Me2	–	–	–	–
H4-K20Me1	–	–	–	–

The data in this table were collected by MALDI-TOF mass spectrometry. In each condition 5–7 μg of purified protein (1–350 aa) was added to each reaction (see Experimental Procedures). In each case, 10 μM of peptide for the indicated modifications was added to the reaction at 37°C for 2–5 hr. Each experiment was conducted at least two independent times.
[a] This activity was only observed with 75 μg of protein.

Keogh et al., 2005). Enzymes that are responsible for trimethylation at many of these sites have been identified (as reviewed in Margueron et al. [2005]; Sun et al., 2005; Zhang and Reinberg, 2001). However, virtually nothing was known about the trimethylation dynamics associated with these or other methylated histones in eukaryotes. The identification of the H3-K9 and H3-K36 trimethyl demethylases in this study supports the dynamic nature of regulation of histone trimethylation. In the case of the transcriptional corepressor JMJD2A, its ability to demethylate H3-K36Me3 and H3-K9Me3 suggests its involvement in transcriptional and posttranscriptional regulation. The role of JMJD2A in these processes may be in addition to, or separate from, the repression activity associated with the recruitment of Rb or the corepressor N-CoR described previously (Gray et al., 2005; Yoon et al., 2003; Zhang et al., 2005).

The ability of JMJD2A to demethylate both H3-K9Me3 and H3-K36Me3 was somewhat unexpected, given that both LSD1 and JHDM1 are highly site specific. Impor-

tantly, the cell culture and *C. elegans* results provided in vivo evidence supporting this possibility (Figures 4–6; Table 1). However, it remains to be determined whether JMJD2A (and JMJD2C) may kinetically favor one site over the other in vivo. In addition, one can not exclude the possibility that these proteins may display altered site specificities in vivo when complexed with different proteins, as has been reported for LSD1 (Metzger et al., 2005; Shi et al., 2005).

Mass spectrometry analysis indicated that JMJD2A converts H3-K9/36Me3 to H3-K9/36Me2 but not H3-K9/36Me1 or unmethylated products (Figures 2 and 3). Thus, a decrease in trimethylation in vivo is predicted to result in an increase in dimethylation at the same site. We observe a slight increase in H3-K9/K36Me2 levels in the JMJD2A-transfected cells; however, we did not detect changes in vitro with bulk histones (Table 1; Figure 3B). When considering mass spectrometric data from human, mouse, and *Drosophila*, these observations may not be that surprising because H3-K9Me2 constitutes as much as 50% of the methylated H3, while mono- and trimethylation represent only 15%–20% for H3 lysine 9 (McKittrick et al., 2004; Peters et al., 2003; Thomas et al., 2006; Zhang et al., 2004). Therefore, a decrease in trimethylation would not necessarily lead to an increase in dimethylation at the same site that is easily detectable by Western blot analysis in vitro. Finally, in vivo we cannot exclude the possibility that JMJD2A may be associated with additional demethylases that can convert the di- to mono- or even to unmodified products.

Fine-Tuning Histone Methylation by Demethylases?

Although the JMJD2 family members all appear to be specific for trimethylated lysine residues, they display differential ability to mediate different degrees of demethylation. Specifically, while JMJD2A/C generates H3-K9Me2, JMJD2D is capable of reducing H3-K9Me3 to the monomethylated state. Although it is formally possible that these differences may represent in vitro peculiarities, we believe that they provide an important mechanism for fine-tuning methylation regulation in vivo. Similar to the JMJD2 demethylases, there are histone methyltransferases that seem to have different capabilities in adding one to three methyl groups per lysine (Kouzarides, 2002; Lachner and Jenuwein, 2002; Margueron et al., 2005; Zhang and Reinberg, 2001). Importantly, loss of the H3-K9Me3-specific methylase Suv39h results in the specific accumulation of H3-K9Me1, while a loss of G9a causes a loss of mono- and dimethylation and but retention of trimethylation, consistent with the potential importance of differential methylation states at the same lysine residue (Peters et al., 2001; Rice et al., 2003). In addition, previous studies have documented that differential methylation levels at the same sites appear to be associated with different chromosomal regions. For instance, H3-K27Me3 is associated with an inactive X chromosome (Fong et al., 2002; Kelly et al., 2002; Reuben and Lin, 2002; Plath et al., 2003; Rougeulle et al., 2004), but H3-K27Me1 is

enriched at pericentric heterochromatin on mitotic chromosomes (Peters et al., 2003). While H3-K9Me3 is also linked to pericentric heterochromatin, H3-K9Me1 and H3-K9Me2 are associated with euchromatin silent domains (Peters et al., 2003; Rice et al., 2003).

Recently, Vakoc et al. (2005) demonstrated that transcriptionally active genes had increased levels of H3-K9Me3 in their coding regions. This observation is consistent with the observed increase of HP1 and H3-K9Me3 staining in heat-shocked genes in *Drosophila* polytenes (Piacentini et al., 2003). These data suggest a correlation between H3-K9 trimethylation and active gene transcription. Previous studies linked H3-K36Me2/Me3 to transcriptional elongation (Krogan et al., 2003; Li et al., 2003; Schaft et al., 2003; Xiao et al., 2003). More recent studies show that H3-K36 methylation is linked to suppression of inappropriate transcription within the body of genes, via recruitment of a specific deacetylase complex (Carrozza et al., 2005; Joshi and Struhl, 2005; Keogh et al., 2005). This mechanism may be important for resetting the chromatin structure to the basal, repressed transcriptional state. Additionally, di- and trimethylated H3-K36 have also shown to be enriched proximal to the 5′ start position of actively transcribed genes and continuing through the 3′ end in both yeast and chicken, suggesting a role for H3-K36 methylation in transcriptional termination and 3′ processing (Bannister et al., 2005; Rao et al., 2005). Therefore, fine tuning methylation at H3-K36, along with H3-K9, could play a fundamental role in both transcriptional and posttranscriptional regulation of gene expression. Future experiments to identify the genomic locations of JMJD2A and its downstream target genes will begin to elucidate the mechanisms by which this class of demethylases function.

Although the exact functions of differentially methylated states are still incompletely understood, the available evidence points to them being an important nexus to an increased regulatory potential associated with histone methylation (Schotta et al., 2004a). The balance between the site-specific methylases and demethylases is expected to generate a whole array of methylation states at various histone lysine residues, which are likely to serve as docking sites for different effector proteins or as altered substrates for both chromatin modifying and remodeling enzymes (e.g., histone deacetylases and methyltransferases).

Histone Methylation/Demethylation and Their Biological Significance

Histone methylation occurs in a host of organisms, ranging from *Neurospora crassa* to *C. elegans* and to humans. Studies in mice have demonstrated that during fertilization and zygotic development H3-K9 methylation undergoes dynamic changes (Sarmento et al., 2004; Yeo et al., 2005). Similarly, *C. elegans* show temporal regulation of H3 methylation, where methylation is absent at certain developmental windows during embryogenesis but returns as animals mature and approach the reproductive stage

(i.e., K4Me3 in germline precursors; Schaner et al., 2003; Schaner, 2006). In addition to a role in embryonic development, methylation is also intricately associated with the silencing of the X chromosome and euchromatic regions in a number of organisms (Cowell et al., 2002; Lucchesi et al., 2005; Rice et al., 2003; Peters et al., 2003).

H3-K9 modification has been observed associated with a transcriptionally silent X chromosome (Kelly et al., 2002; Reuben and Lin, 2002; Rougeulle et al., 2004). However, H3-K36 methylation on the X chromosome has not been analyzed. Our finding that ceJMJD2 suppresses H3-K36Me3 on the X chromosome suggests that keeping low, infrequent levels of K36Me3 on the X chromosome may be important for maintaining low gene expression during germline development (Kelly et al., 2002; Reinke et al., 2000; Reuben and Lin, 2002). Similarly, other activating marks H3-K4Me2/Me3 are absent on the *C. elegans* X chromosome until diplotene region and diakinetic oocytes (Kelly et al., 2002; Schaner et al., 2003; Schaner, 2006), emphasizing the importance of histone methylation regulation during development.

Another important finding of this study is that overall H3-K9Me3 signal increases in the *C. elegans* germline upon depletion by RNAi, which is paralleled by an increase in apoptosis. In *C. elegans*, DNA damage-induced apoptosis is genetically distinct from either somatic cell death or physiological germ cell death (Gartner et al., 2000; Gumienny et al., 1999; Stergiou and Hengartner, 2004). Moreover, DNA damage-induced apoptosis requires the p53 homolog, CEP-1, and often accompanies increased RAD-51 foci levels, which is what we have observed in the *ceJMJD2 (RNAi)* animals (Derry et al., 2001; Schumacher et al., 2001, 2005; Colaiacovo et al., 2003). These data suggest a link to DNA damage-induced apoptosis; however, the exact mechanism underlying these observations requires further investigation. Our findings suggest that an imbalance of histone methylation at H3-K9 and possibly H3-K36 may provide an altered chromatin environment that would affect repair either through increased DSBs, delayed repair kinetics of break-dependent recombination intermediates, and/or through downstream transcriptional targets involved in DNA-damage repair. These observations raise the possibility that alterations of the expression and/or activities of the JMJD2 family members may contribute to human diseases such as cancer. Consistent with this hypothesis, the *JMJD2C* gene (also called GASC-1; Yang et al., 2000) is often amplified in squamous cell carcinoma and desmoplastic medulloblastoma (Ehrbrecht et al., 2006). Such a hypothesis is also supported by the recent studies that implicate histone methylation regulation in tumorigenesis (Canaani et al., 2004; Fraga et al., 2005; Hess, 2004b; Jaju et al., 2001; Pogribny et al., 2006). Collectively, these findings suggest that both methylases and demethylases may play important roles in tumorigenesis. Therefore, the identification of histone demethylases provides the opportunity to investigate the relationship of this ever-growing family of histone modifying enzymes in development and human cancers.

EXPERIMENTAL PROCEDURES

Expression Constructs

hJMJD2A was PCR amplified from HeLa cell cDNA using Platinum Pfx polymerase (Invitrogen) and introduced into the Gateway Entry system. A fully sequenced cDNA, as well as the H188A catalytic mutant generated by PCR of this cDNA, were transferred into additional Gateway vectors: HA-tag and FLAG-baculovirus. The first 350 amino acids for hJMJD2A were subcloned into the pGEX-4T2 expression construct, expressed, and purified with GST beads. The cDNA corresponding to the first 350 amino acids for JMJD2B, -2C, and -2D were amplified from a mixed cDNA library using the GC-Rich kit (Roche) and Tgo polymerase (Roche), subcloned into pET28a and sequenced before being transformed and expressed from Rosetta cells. The HIS-tagged proteins were purified by Ni-NTA affinity resin (Qiagen). The NTA beads were washed with 20 mM imidazole before being eluted in 250 mM inidazole. The purified proteins were then dialyzed in DeMTase buffer 1 (20 mM Tris-HCl [pH 7.3], 150 mM NaCl, 8.0% glycerol, 1 mM DTT, 1 mM PMSF).

Demethylation Reactions

Purified proteins were incubated with 10 μM of peptide or 5 μg of calf thymus type II-A histones (Sigma) in the DeMTase reaction buffer 1 (20 mM Tris-HCl [pH 7.3], 150 mM NaCl, 50 μM $(NH_4)_2Fe(SO_4)_2$ + $6(H_2O)$, 1 mM α-ketoglutarate, and 2 mM ascorbic acid) for 2–5 hr at 37°C. A total of 1–2 μg of full-length hJMJD2A or 1–7.5 μg of the N/C domains for JMJD2A-D were added to the reactions. The reactions were inhibited by 10 μM EDTA and 250 μM DFO (Sigma-Aldrich).

MALDI-TOF Mass Spectrometry

One microliter of the 100 μl demethylation reaction mixture was desalted through a C18 ZipTip (Millipore). The ZipTip was activated, equilibrated, and loaded as previously described by Shi et al. (2004). The bound material was then eluted with 10 mg/ml α-cyano-4-hydroxycinnamic acid MALDI matrix in 70% acetonitrile/0.1% TFA before being spotted and cocrystallized. The samples were analyzed by a MALDI-TOF/TOF mass spectrometer (Waters) in Hidde Ploegh's Mass Spectrometry facility at the Whitehead Institute (Cambridge, MA).

Cell Culture and Transfections

HeLa (ATCC) cells were cultured in DMEM (Invitrogen) supplemented with 10% Fetalplex, 1X penicillin/streptomycin, and L-glutamine at 37°C and 5% CO_2. HeLa cells were plated on coverslips in 24-well dishes (2.5 $\times$ 10^4 cells/well) and transfected with Lipofectamine 2000 according to the manufacturer's instructions.

Immunofluorescence Microscopy

Seventy-two hours posttransfection (i.e., HA-JMJD2A and HA-JMJD2A H188A), cells were fixed with 3% paraformaldehyde, permeabilized, and blocked (10% FBS). The coverslip was incubated for 3 hr at room temperature with the appropriate primary antibody, which was then washed and incubated with the corresponding secondary antibodies for 1 hr at room temperature. The coverslips were then washed, mounted with Vectashield (Vector Laboratories), and analyzed by fluorescence microscopy (Leica) using a 60× objective. Images were acquired and processed with Openlab 3.1.5 software. Primary antibodies were used at the following dilutions: 1:1000 anti-HA (Covance monoclonal HA.11), 1:1000 anti-monomethyl H3-K4 (Upstate 07-436), 1:160000 anti-dimethyl H3-K4 (Upstate 07-030), 1:20000 anti-trimethyl H3-K4 (Upstate 07-473), 1:5000 anti-monomethyl H3-K9 (Upstate 07-450), 1:5000 anti-dimethyl H3-K9 (Upstate 07-441), 1:5000 anti-trimethyl H3-K9 (Upstate 07-442), 1:10000 anti-monomethyl H3-K36 (Abcam 9048), 1:5000 anti-dimethyl H3-K36 (Upstate 07-274), 1:5000 anti-trimethyl H3-K36 (Abcam 9050). Donkey-anti-rabbit (Molecular Probes Alexa 594) and goat-anti-mouse (Molecular Probes Alexa 488) secondary antibodies were used at 1:2000. DAPI was used with all staining. The cells were scored based

on a moderately high to high level of expression, which is reflected in Figure 4. The cells that were not positive for HA staining were used as background controls.

General Worm Culture and Strains

Bristol N2 and cep-1 (lg12501) (Schumacher et al., 2005) worms were utilized. C. elegans strains were cultured at 25°C under standard conditions as described by Brenner (1974).

C. elegans Immunostaining

DAPI staining and immunostaining of C. elegans germlines from both ceJMJD2 (RNAi) and control (RNAi) age-matched worms were carried out as described in Colaiacovo et al., (2003). Primary antibodies were used at the following dilutions: 1:1000 for anti-trimethyl H3-K36 (H3-K36Me3; Abcam 9050) and anti-trimethyl H3-K9 (H3-K9Me3; Upstate 07-442); 1:100 for anti-RAD-51 (a rabbit antisera described in Colaiacovo et al. [2003]). Cy3 anti-rabbit (Jackson Immunochemicals) secondary was utilized at 1:100. Images are projections halfway through 3D data stacks of whole nuclei. Optical sections were collected at 0.2 μm intervals utilizing a Delta Vision deconvolution microscope.

C. elegans Apoptosis Assay

Germlines were examined both by acridine orange staining and Nomarski optics as in Kelly et al. (2000). The images shown in Figure 5 were acquired with a Leica DM5000 B microscope (60× objective) and processed with Openlab 3.1.5 software. Germ cell corpses were scored in adult hermaphrodites 54–56 hr after being plated as L1 larvae on RNAi food or HB101 bacteria, corresponding to the same relative age assayed by Kelly et al. (2000). The apoptosis data represent six experimental data sets. A total of 109 gonad arms were scored for control (RNAi) (362 germ cell corpses/109 gonads), a total of 121 gonad arms for ceJMJD2 (RNAi) (1118 germ cell corpses/ 121 gonads), a total of 54 gonad arms for cep-1 (lg12501); control (RNAi) (170 germ cell corpses/54 gonads), and a total of 55 gonad arms for cep-1 (lg12501); ceJMJD2 (RNAi) (193 germ cell corpses/55 gonads). Statistical comparisons between these genetic backgrounds were conducted using the two-tailed Mann-Whitney test. ceJMJD2 (RNAi) differed significantly from the control (RNAi), from cep-1 (lg12501); control (RNAi), and from cep-1 (lg12501); ceJMJD2(RNAi) (p = < 0.0001), whereas cep-1 (lg12501); ceJMJD2 (RNAi) did not differ from either control (RNAi) or cep-1 (lg12501); control (RNAi) (p = 0.6885 and p = 0.3887, respectively). The statistical analysis was performed using InStat3 software (http://www.graphpad.com).

Analysis of Immunostained C. elegans Meiotic Nuclei

Following image acquisition, the germlines were divided into seven (36 μm $\times$ 36 μm) zones as in Martinez-Perez and Villeneuve, (2005) (Figure S4B). This allowed both for an inspection of the various antibody localization patterns observed throughout meiotic prophase, as well as for a reproducible quantitative analysis of levels of staining within particular stages of meiotic prophase. The data presented for anti-H3-K9Me3 in Figure 5 was from two experimental data sets. A total of 81 and 56 different gonad arms were examined for ceJMJD2 (RNAi) and control (RNAi), respectively. Specifically, the late pachytene zone (zone 7) was examined for the anti-H3-K9Me3 immunostaining (Figures 5A and 5B). This corresponds to the zone where increased levels of germ cell corpses are observed due to the activation of a late-pachytene DNA-damage checkpoint (Colaiacovo et al., 2003; Gartner et al., 2000; MacQueen et al., 2002) and corresponds to the region where we observed the intensely H3-K9Me3-stained nuclei. The data presented for H3-K36me3 corresponds to a total of 117 and 123 nuclei scored within the nine ceJMJD2 (RNAi) and control (RNAi) germlines, respectively.

The data presented for anti-RAD-51 consists of a total of 165 and 184 nuclei scored for ceJMJD2 (RNAi) and control (RNAi) germlines, respectively. The mid-pachytene zone (zone 5) was selected for scoring levels of RAD-51 foci given that this zone is where both the total

numbers of nuclei carrying RAD-51 foci and the numbers of RAD-51 foci/nucleus are the highest in N2 (Colaiacovo et al., 2003).

Supplemental Data

Supplemental Data include five figures, one table, and Supplemental Experimental Procedures and can be found with this article online at http://www.cell.com/cgi/content/full/125/3/467/DC1/.

REFERENCES

Alpi, A., Pasierbek, P., Gartner, A., and Loidl, J. (2003). Genetic and cytological characterization of the recombinant protein RAD-51 in *Caenorhabditis elegans*. Chromosoma *112*, 6–16.

Bannister, A.J., Schneider, R., Myers, F.A., Thorne, A.W., Crane-Robinson, C., and Kouzarides, T. (2005). Spatial distribution of di- and trimethyl lysine 36 of histone H3 at active genes. J. Biol. Chem. *280*, 17732–17736.

Bean, C.J., Schaner, C.E., and Kelly, W.G. (2004). Meiotic pairing and imprinted X chromatin assembly in Caenorhabditis elegans. Nat. Genet. *36*, 100–105.

Brenner, S. (1974). The genetics of Caenorhabditis elegans. Genetics *77*, 71–94.

Byvoet, P., Shepherd, G.R., Hardin, J.M., and Noland, B.J. (1972). The distribution and turnover of labeled methyl groups in histone fractions of cultured mammalian cells. Arch. Biochem. Biophys. *148*, 558–567.

Canaani, E., Nakamura, T., Rozovskaia, T., Smith, S.T., Mori, T., Croce, C.M., and Mazo, A. (2004). ALL-1/MLL1, a homologue of Drosophila TRITHORAX, modifies chromatin and is directly involved in infant acute leukaemia. Br. J. Cancer *90*, 756–760.

Carrozza, M.J., Li, B., Florens, L., Suganuma, T., Swanson, S.K., Lee, K.K., Shia, W.-J., Anderson, S., Yates, J., Washburn, M.P., and Workman, J.L. (2005). Histone H3 methylation by SET2 directs deacetylation of coding regions by RPD3S to suppress spurious intragenic transcription. Cell *123*, 581–592.

Clissold, P.M., and Ponting, C.P. (2001). JmjC: cupin metalloenzyme-like domains in jumonji, hairless and phospholipase A2beta. Trends Biochem. Sci. *26*, 7–9.

Colaiacovo, M.P., MacQueen, A.J., Martinez-Perez, E., McDonald, K., Adamo, A., La Volpe, A., and Villeneuve, A.M. (2003). Synaptonemal complex assembly in C. elegans is dispensable for loading strand-exchange proteins but critical for proper completion of recombination. Dev. Cell *5*, 463–474.

Cowell, I.G., Aucott, R., Mahadevaiah, S.K., Burgoyne, P.S., Huskisson, N., Bongiorni, S., Prantera, G., Fanti, L., Pimpinelli, S., Wu, R.,

et al. (2002). Heterochromatin, HP1 and methylation at lysine 9 of histone H3 in animals. Chromosoma *111*, 22–36.

Derry, W.B., Putzke, A.P., and Rothman, J.H. (2001). Caenorhabditis elegans p53: role in apoptosis, meiosis, and stress resistance. Science *294*, 591–595.

Ehrbrecht, A., Muller, U., Wolter, M., Hoischen, A., Koch, A., Radlwimmer, B., Actor, B., Mincheva, A., Pietsch, T., Lichter, P., et al. (2006). Comprehensive genomic analysis of desmoplastic medulloblastomas: identification of novel amplified genes and separate evaluation of the different histological components. J. Pathol. *208*, 554–563.

Felsenstein, J. (1989). PHYLIP—Phylogeny inference package (version 3.2). Cladistics *5*, 164–166.

Fong, Y., Bender, L., Wang, W., and Strome, S. (2002). Regulation of the different chromatin states of autosomes and X chromosomes in the germ line of C. elegans. Science *296*, 2235–2238.

Fraga, M.F., Ballestar, E., Villar-Garea, A., Boix-Chornet, M., Espada, J., Schotta, G., Bonaldi, T., Haydon, C., Ropero, S., Petrie, K., et al. (2005). Loss of acetylation at lys 16 and trimethylation at lys 20 of histone H4 is a common hallmark of human cancer. Nat. Genet. *37*, 391–400.

Gartner, A., Milstein, S., Ahmed, S., Hodgkin, J., and Hengartner, M.O. (2000). A conserved checkpoint pathway mediates DNA damage-induced apoptosis and cell cycle arrest in *C. elegans*. Mol. Cell *5*, 435–443.

Gray, S.G., Iglesias, A.H., Lizcano, F., Villanueva, R., Camelo, S., Jingu, H., Teh, B.T., Koibuchi, N., Chin, W.W., Kokkotou, E., and Dangond, F. (2005). Functional characterization of JMJD2A, a histone deacetylase- and retinoblastoma-binding protein. J. Biol. Chem. *280*, 28507–28518.

Gumienny, T.L., Lambie, E., Hartwieg, E., Horvitz, H.R., and Hengartner, M.O. (1999). Genetic control of programmed cell death in the Caenorhabditis elegans hermaphrodite germline. Development *126*, 1011–1022.

Hake, S.B., Xiao, A., and Allis, C.D. (2004). Linking the epigenetic 'language' of covalent histone modifications to cancer. Br. J. Cancer *90*, 761–769.

Hess, J.L. (2004a). Mechanisms of transformation by MLL. Crit. Rev. Eukaryot. Gene Expr. *14*, 235–254.

Hess, J.L. (2004b). MLL: a histone methyltransferase disrupted in leukemia. Trends Mol. Med. *10*, 500–507.

Jaju, R.J., Fidler, C., Haas, O.A., Strickson, A.J., Watkins, F., Clark, K., Cross, N.C., Cheng, J.F., Aplan, P.D., Kearney, L., et al. (2001). A novel gene, NSD1, is fused to NUP98 in the t(5;11)(q35;p15.5) in de novo childhood acute myeloid leukemia. Blood *98*, 1264–1267.

Jenuwein, T., and Allis, C.D. (2001). Translating the histone code. Science *293*, 1074–1080.

Joshi, A.A., and Struhl, K. (2005). Eaf3 chromodomain interaction with methylated H3-K36 links histone deacetylation to Pol II elongation. Mol. Cell *20*, 971–978.

Katoh, M. (2004). Identification and characterization of JMJD2 family genes in silico. Int. J. Oncol. *24*, 1623–1628.

Kelly, K.O., Dernburg, A.F., Stanfield, G.M., and Villeneuve, A.M. (2000). Caenorhabditis elegans msh-5 is required for both normal and radiation-induced meiotic crossing over but not for completion of meiosis. Genetics *156*, 617–630.

Kelly, W.G., Schaner, C.E., Dernburg, A.F., Lee, M.H., Kim, S.K., Villeneuve, A.M., and Reinke, V. (2002). X-chromosome silencing in the germline of C. elegans. Development *129*, 479–492.

Keogh, M.C., Kurdistani, S.K., Morris, S.A., Ahn, S.H., Podolny, V., Collins, S.R., Schuldiner, M., Chin, K., Punna, T., Thompson, N.J., et al. (2005). Cotranscriptional set2 methylation of histone H3 lysine 36 recruits a repressive Rpd3 complex. Cell *123*, 593–605.

Kim, J., Daniel, J., Espejo, A., Lake, A., Krishna, M., Xia, L., Zhang, Y., and Bedford, M.T. (2006). Tudor, MBT and chromo domains gauge the degree of lysine methylation. EMBO Rep., in press. Published online January 13, 2006. 10.1038/sj.embor.7400625.

Kouzarides, T. (2002). Histone methylation in transcriptional control. Curr. Opin. Genet. Dev. 12, 198–209.

Krogan, N.J., Kim, M., Tong, A., Golshani, A., Cagney, G., Canadien, V., Richards, D.P., Beattie, B.K., Emili, A., Boone, C., et al. (2003). Methylation of histone H3 by SET2 in Saccharomyces cerevisiae is linked to transcriptional elongation by RNA Polymerase II. Mol. Cell. Biol. 23, 4207–4218.

Lachner, M., and Jenuwein, T. (2002). The many faces of histone lysine methylation. Curr. Opin. Genet. Dev. 14, 286–298.

Lee, C., Kim, S.J., Jeong, D.G., Lee, S.M., and Ryu, S.E. (2003). Structure of human FIH-1 reveals a unique active site pocket and interaction sites for HIF-1 and von Hippel-Lindau. J. Biol. Chem. 278, 7558–7563.

Lee, M.G., Wynder, C., Cooch, N., and Shiekhattar, R. (2005). An essential role for CoREST in nucleosomal histone 3 lysine 4 demethylation. Nature 437, 432–435.

Li, B., Howe, L., Anderson, S., Yates, J.R., III, and Workman, J.L. (2003). The SET2 histone methyltransferase functions through the phosphorylated carboxyl-terminal domain of RNA polymerase II. J. Biol. Chem. 278, 8897–8903.

Lucchesi, J.C., Kelly, W.G., and Panning, B. (2005). Chromatin remodeling in dosage compensation. Annu. Rev. Genet. 39, 615–651.

MacQueen, A.J., Colaiacovo, M.P., McDonald, K., and Villeneuve, A.M. (2002). Synapsis-dependent and -independent mechanisms stabilize homolog pairing during meiotic prophase in C. elegans. Genes Dev. 16, 2428–2442.

Margueron, R., Trojer, P., and Reinberg, D. (2005). The key to development: interpreting the histone code? Curr. Opin. Genet. Dev. 15, 163–176.

Martin, C., and Zhang, Y. (2005). The diverse functions of histone lysine methylation. Nat. Rev. Mol. Cell Biol. 6, 838–849.

Martinez-Perez, E., and Villeneuve, A.M. (2005). HTP-1-dependent constraints coordinate homolog pairing and synapsis and promote chiasma formation during C. elegans meiosis. Genes Dev. 19, 2727–2743.

McKittrick, E., Gafken, P.R., Ahmad, K., and Henikoff, S. (2004). Histone H3.3 is enriched in covalent modifications associated with active chromatin. Proc. Natl. Acad. Sci. USA 101, 1525–1530.

Metzger, E., Wissmann, M., Yin, N., Muller, J.M., Schneider, R., Peters, A.H., Gunther, T., Buettner, R., and Schule, R. (2005). LSD1 demethylates repressive histone marks to promote androgen-receptor-dependent transcription. Nature 437, 436–439.

Nakayama, J.-I., Rice, J.C., Strahl, B.D., Allis, C.D., and Grewal, S.I.S. (2001). Role of histone H3 lysine 9 methylatin in epigenetic control of heterochromatin assembly. Science 292, 110–113.

Nielsen, S.J., Schneider, R., Bauer, U.M., Bannister, A.J., Morrison, A., O'Carroll, D., Firestein, R., Cleary, M., Jenuwein, T., Herrera, R.E., and Kouzarides, T. (2001). Rb targets histone H3 methylation and HP1 to promoters. Nature 412, 561–565.

Okada, Y., Feng, Q., Lin, Y., Jiang, Q., Li, Y., Coffield, V.M., Su, L., Xu, G., and Zhang, Y. (2005). hDOT1L links histone methylation to leukemogenesis. Cell 121, 167–178.

Peters, A.H., O'Carroll, D., Scherthan, H., Mechtler, K., Sauer, S., Schofer, C., Weipoltshammer, K., Pagani, M., Lachner, M., Kohlmaier, A., et al. (2001). Loss of the Suv39h histone methyltransferases impairs mammalian heterochromatin and genome stability. Cell 107, 323–337.

Peters, A.H., Mermoud, J.E., O'Carroll, D., Pagani, M., Schweizer, D., Brockdorff, N., and Jenuwein, T. (2002). Histone H3 lysine 9 methylation is an epigenetic imprint of facultative heterochromatin. Nat. Genet. 30, 77–80.

Peters, A.H., Kubicek, S., Mechtler, K., O'Sullivan, R.J., Derijck, A.A., Perez-Burgos, L., Kohlmaier, A., Opravil, S., Tachibana, M., Shinkai, Y., et al. (2003). Partitioning and plasticity of repressive histone methylation states in mammalian chromatin. Mol. Cell 12, 1577–1589.

Piacentini, L., Fanti, L., Berloco, M., Perrini, B., and Pimpinelli, S. (2003). Heterochromatin protein 1 (HP1) is associated with induced gene expression in Drosophila euchromatin. J. Cell Biol. 161, 707–714.

Plath, K., Fang, J., Mlynarczyk-Evans, S.K., Cao, R., Worringer, K.A., Wang, H., de la Cruz, C.C., Otte, A.P., Panning, B., and Zhang, Y. (2003). Role of histone H3 lysine 27 methylation in X inactivation. Science 300, 131–135.

Pogribny, I.P., Ross, S.A., Tryndyak, V.P., Pogribna, M., Poirier, L.A., and Karpinets, T.V. (2006). Histone H3 lysine 9 and H4 lysine 20 trimethylation and the expression of Suv4–20h2 and Suv-39h1 histone methyltransferases in hepatocarcinogenesis induced by methyl deficiency in rats. Carcinogenesis, in press. Published online February 23, 2006. 10.1093/carcin/bgi364.

Rao, B., Shibata, Y., Strahl, B.D., and Lieb, J.D. (2005). Dimethylation of histone H3 at lysine 36 demarcates regulatory and nonregulatory chromatin genome-wide. Mol. Cell. Biol. 25, 9447–9459.

Rea, S., Eisenhaber, F., O'Carroll, D., Strahl, B.D., Sun, Z.-W., Opravil, S., Mechtier, K., Ponting, C.P., Allis, C.D., and Jenuwein, T. (2000). Regulation of chromatin structure by site-specific histone H3 methyltransferases. Nature 406, 593–599.

Reinke, V., Smith, H.E., Nance, J., Wang, J., Van Doren, C., Begley, R., Jones, S.J., Davis, E.B., Scherer, S., Ward, S., and Kim, S.K. (2000). A global profile of germline gene expression in C. elegans. Mol. Cell 6, 605–616.

Reuben, M., and Lin, R. (2002). Germline X chromosomes exhibit contrasting patterns of histone H3 methylation in Caenorhabditis elegans. Dev. Biol. 245, 71–82.

Rice, J.C., Briggs, S.D., Ueberheide, B., Barber, C.M., Shabanowitz, J., Hunt, D.F., Shinkai, Y., and Allis, C.D. (2003). Histone methyltransferases direct different degrees of methylation to define distinct chromatin domains. Mol. Cell 12, 1591–1598.

Rinaldo, C., Ederle, S., Rocco, V., and La Volpe, A. (1998). The Caenorhabditis elegans RAD-51 homolog is transcribed into two alternative mRNAs potentially encoding proteins of different sizes. Mol. Gen. Genet. 260, 289–294.

Rougeulle, C., Chaumeil, J., Sarma, K., Allis, C.D., Reinberg, D., Avner, P., and Heard, E. (2004). Differential histone H3 Lys-9 and Lys-27 methylation profiles on the X chromosome. Mol. Cell. Biol. 24, 5475–5484.

Sanders, S.L., Portoso, M., Mata, J., Bahler, J., Allshire, R.C., and Kouzarides, T. (2004). Methylation of histone H4 lysine 20 controls recruitment of Crb2 to sites of DNA damage. Cell 119, 603–614.

Sarmento, O.F., Digilio, L.C., Wang, Y., Perlin, J., Herr, J.C., Allis, C.D., and Coonrod, S.A. (2004). Dynamic alterations of specific histone modifications during early murine development. J. Cell Sci. 117, 4449–4459.

Schaft, D., Roguev, A., Kotovic, K.M., Shevchenko, A., Sarov, M., Shevchenko, A., Neugebauer, K.M., and Stewart, A.F. (2003). The histone 3 lysine 36 methyltransferase, SET2, is involved in transcriptional elongation. Nucleic Acids Res. 31, 2475–2482.

Schaner, C.E. and Kelly, W.G. (2006). Germline chromatin. WormBook, ed. The C elegans Research Community, WormBook. Published online January 24, 2006. 10.1895/wormbook.1.73.1. http://www.wormbook.org.

Schaner, C.E., Deshpande, G., Schedl, P.D., and Kelly, W.G. (2003). A conserved chromatin architecture marks and maintains the restricted germ cell lineage in worms and fliers. Dev. Cell 5, 747–757.

Schneider, R., Bannister, A.J., and Kouzarides, T. (2002). Unsafe SETs: histone lysine methyltransferases and cancer. Trends Biochem. Sci. *27*, 396–402.

Schotta, G., Lachner, M., Peters, A.H., and Jenuwein, T. (2004a). The indexing potential of histone lysine methylation. Novartis Found. Symp. *259*, 22–37; discussion 37–47, 163–169.

Schotta, G., Lachner, M., Sarma, K., Ebert, A., Sengupta, R., Reuter, G., Reinberg, D., and Jenuwein, T. (2004b). A silencing pathway to induce H3–K9 and H4–K20 trimethylation at constitutive heterochromatin. Genes Dev. *18*, 1251–1262.

Schumacher, B., Hofmann, K., Boulton, S., and Gartner, A. (2001). The *C. elegans* homolog of the p53 tumor suppressor is required for DNA damage-induced apoptosis. Curr. Biol. *11*, 1722–1727.

Schumacher, B., Hanazawa, M., Lee, M.H., Nayak, S., Volkmann, K., Hofmann, E.R., Hengartner, M., Schedl, T., and Gartner, A. (2005). Translational repression of *C. elegans* p53 by GLD-1 regulates DNA damage-induced apoptosis. Cell *120*, 357–368.

Shi, Y., Lan, F., Matson, C., Mulligan, P., Whetstine, J.R., Cole, P.A., Casero, R.A., and Shi, Y. (2004). Histone demethylation mediated by the nuclear amine oxidase homolog LSD1. Cell *119*, 941–953.

Shi, Y.J., Sawada, J.-I., Sui, G.C., Affar, E.B., Whetstine, J., Lan, F., Ogawa, H., Luke, M.P.-S., Nakatani, Y., and Shi, Y. (2003). Coordinated histone modifications mediated by a CtBP co-repressor complex. Nature *422*, 735–738.

Shi, Y.J., Matson, C., Lan, F., Iwase, S., Baba, T., and Shi, Y. (2005). Regulation of LSD1 histone demethylase activity by its associated factors. Mol. Cell *19*, 857–864.

Stergiou, L., and Hengartner, M.O. (2004). Death and more: DNA-damage response pathways in the nematode C. elegans. Cell Death Differ. *11*, 21–28.

Strahl, B.D., and Allis, C.D. (2000). The language of covalent histone modifications. Nature *403*, 41–45.

Sun, X.J., Wei, J., Wu, X.Y., Hu, M., Wang, L., Wang, H.H., Zhang, Q.H., Chen, S.J., Huang, Q.H., and Chen, Z. (2005). Identification and characterization of a novel human histone H3 lysine 36-specific methyltransferase. J. Biol. Chem. *280*, 35261–35271.

Sung, P. (1994). Catalysis of ATP-dependent homologous DNA pairing and strand exchange by yeast RAD51 protein. Science *265*, 1241–1243.

Takanami, T., Sato, S., Ishihara, T., Katsura, I., Takahashi, H., and Higashitani, A. (1998). Characterization of a Caenorhabditis elegans recA-like gene Ce-rdh-1 invovled in meiotic recombination. DNA Res. *5*, 373–377.

Thomas, G., Lange, H.W., and Hempel, K. (1972). Relative stability of lysine-bound methyl groups in arginine-rich histones and their subfractions in Ehrlich ascites tumor cells in vitro. Hoppe Seylers Z. Physiol. Chem. *353*, 1423–1428.

Thomas, C.E., Kelleher, N.L., and Mizzen, C.A. (2006). Mass spectrometric characterization of human histone H3: a bird's eye view. J. Proteome Res. *5*, 240–247.

Tsukada, Y., Fang, J., Erdjument-Bromage, H., Warren, M.E., Borchers, C.H., Tempst, P., and Zhang, Y. (2006). Histone demethylation by a family of JmjC domain-containing proteins. Nature *439*, 811–816.

Vakoc, C.R., Mandat, S.A., Olenchock, B.A., and Blobel, G.A. (2005). Histone H3 lysine 9 methylation and HP1gamma are associated with transcription elongation through mammalian chromatin. Mol. Cell *19*, 381–391.

Varambally, S., Dhanasekaran, S.M., Zhou, M., Barrette, T.R., Kumar-Sinha, C., Sanda, M.G., Ghosh, D., Pienta, K.J., Sewalt, R.G.A.B., Otte, A.P., et al. (2002). The polycomb group protein EZH2 is involved in progression of prostate cancer. Nature *419*, 624–629.

Xiao, T., Hall, H., Kizer, K.O., Shibata, Y., Hall, M.C., Borchers, C.H., and Strahl, B.D. (2003). Phosphorylation of RNA polymerase II CTD regulates H3 methylation in yeast. Genes Dev. *17*, 654–663.

Yang, Z.Q., Imoto, I., Fukuda, Y., Pimkhaokham, A., Shimada, Y., Imamura, M., Sugano, S., Nakamura, Y., and Inazawa, J. (2000). Identification of a novel gene, GASC1, within an amplicon at 9p23–24 frequently detected in esophageal cancer cell lines. Cancer Res. *60*, 4735–4739.

Yeo, S., Lee, K.K., Han, Y.M., and Kang, Y.K. (2005). Methylation changes of lysine 9 of histone H3 during preimplantation mouse development. Mol. Cells *20*, 423–428.

Yoon, H.G., Chan, D.W., Huang, Z.Q., Li, J., Fondell, J.D., Qin, J., and Wong, J. (2003). Purification and functional characterization of the human N-CoR complex: the roles of HDAC3, TBL1 and TBLR1. EMBO J. *22*, 1336–1346.

Zhang, Y., and Reinberg, D. (2001). Transcriptin regulation by histone methylation: interplay between different covalent modifications of the core histone tails. Genes Dev. *15*, 2343–2360.

Zhang, K., Siino, J.S., Jones, P.R., Yau, P.M., and Bradbury, E.M. (2004). A mass spectrometric "Western blot" to evaluate the correlations between histone methylation and histone acetylation. Proteomics *4*, 3765–3775.

Zhang, D., Yoon, H.G., and Wong, J. (2005). JMJD2A is a novel N-CoR-interacting protein and is involved in repression of the human transcription factor achaete scute-like homologue 2 (ASCL2/Hash2). Mol. Cell. Biol. *25*, 6404–6414.